TECTONICS, VOL. 20, NO. 4, PAGES 474-486, AUGUST 2001

Structure of the Altyn Tagh Fault and Daxue Shan from magnetotelluric surveys: Implications for faulting associated with the rise of the Tibetan Plateau

Paul A. Bedrosian

Geophysics Program, University of Washington, Seattle, Washington

Martyn J. Unsworth

Institute for Geophysical Research, University of Alberta, Edmonton, Alberta

Fei Wang

Beijing Research Institute for Uranium Geology, Beijing, China

Abstract. Magnetotelluric measurements in the foreland of the Daxue Shan have imaged low-angle ($<20°$) thrust faults that extend to a depth of 3 km. The surface projections of the faults at depth coincide with the mapped traces of the Chang Ma (M=7.6, 1932) and North Hills thrusts. Minimum cumulative offsets of 7 km on the Chang Ma thrust and 14 km on the North Hills thrust are estimated from the horizontal extent of underthrust sediment. Assuming that regional thrusting began at 5-6 Ma, this corresponds to minimum convergence rates of 1.3 mm/yr and 2.5 mm/yr on the Chang Ma and North Hills thrusts, respectively. These slip rates correspond to ~ 3 mm/yr of sinistral slip on the Altyn Tagh Fault between 96°E and 97°E. This is consistent with the 4 ± 2 mm/yr of slip estimated by geological studies. Assuming comparable slip rates and similar fault geometry in the neighboring ranges, this requires a minimum of 11 mm/yr of shortening parallel to the Altyn Tagh fault between the Dang He Nan Shan and Qilian Shan. Both the style of thrusting and rate of shortening are in agreement with geologic studies that favor a relatively high rate of slip on the Altyn Tagh fault. This, in turn, implies that lithospheric extrusion contributes significantly in accommodating the ongoing convergence between India and Asia. Farther west, the Altyn Tagh Fault is imaged on four magnetotelluric profiles as a vertical resistivity contrast extending to a depth of at least 8 km. Two strands of the North Altyn Tagh Fault are imaged east of the asperity near Subei (39°30′N, 95°E).

Paper number 2000TC001215.
0278-7407/01/2000TC001215$12.00

1. Introduction

The Tibetan Plateau is the spectacular result of the ongoing India-Asia collision. In the last 20 years it has been the focus of a number of geological and geophysical studies that have sought to understand the processes occurring during compressional orogenesis and plateau formation. Many of the early geophysical and geological studies were focused in southern Tibet where the Indian plate is underthrusting Asia [*Zhao et al.*, 1993; *Allègre et al.*, 1984; *Nelson et al.*, 1996]. Despite these studies many diverse geodynamic models are still tenable explanations of the mode of crustal and mantle deformation in response to the ongoing collision [*Yin and Harrison*, 2000, and references therein].

In particular, the mechanisms that are absorbing the ongoing convergence are not well quantified. *England and Houseman* [1986] and *Dewey and Burke* [1973] suggest that a mass balance can be achieved through north-south compression alone. However, large offsets on the major strike-slip faults within Tibet strongly suggest that significant eastward extrusion of the crust and upper mantle is occurring [*Peltzer and Tapponnier*, 1988; *Tapponnier et al.*, 1982]. Determining the magnitudes of these effects can only be addressed through studies of locations on and around the Tibetan Plateau where these processes are presently active. In the far northeast of the plateau, between the Kunlun and Altyn Tagh Faults, the tectonics is characterized by motion on these strike-slip faults and basin infilling [*Chen et al.*, 1999; *Meyer et al.*, 1998; *Tapponnier et al.*, 1990; *Burchfiel et al.*, 1989]. This region is a young outgrowth of the Tibetan Plateau, and the mechanisms at work today may be similar to those which formed the interior of the present-day plateau [*Meyer et al.*, 1998].

The Altyn Tagh Fault (ATF) bounds the northern edge of the Tibetan Plateau and is over 1200 km in

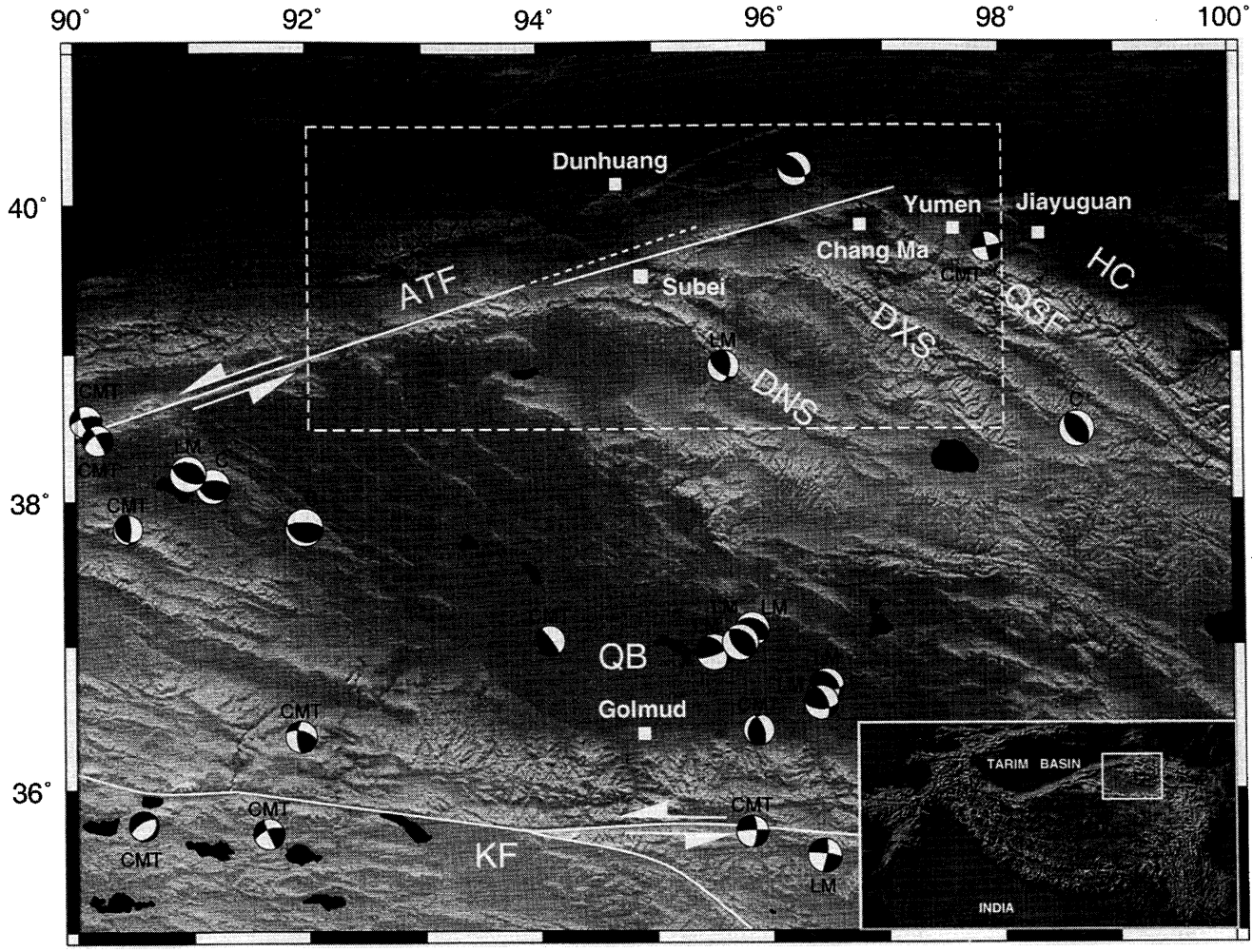

Figure 1. Seismotectonic map of the Qaidam basin and surrounding ranges. Abbreviations are as follows: ATF, Altyn Tagh Fault; KF, Kunlun Fault; QB, Qaidam Basin; DNS, Dang He Nan Shan; DXS, Daxue Shan; QSF, Qilian Shan Front; and HC, Hexi Corridor. The dashed box highlights the region of study shown in Plate 1. Topography is from the *EROS Data Center* [1993]. Focal mechanisms for large earthquakes are shown as lower hemisphere projections of the focal sphere; darkened regions indicate compressional P wave motion. Focal mechanisms are from *Molnar and Lyon-Caen* [1989] (LM), *Chen et al.* [1999] (C), and the centroid moment tensor (CMT) catalog at Harvard University [*Dziewonski et al.*, 1981] (CMT).

length (Figure 1). The eastern segment of the ATF (92°E - 100°E) terminates by branching into multiple, sub parallel strands east of 92°E [*Bayasgalan et al.*, 1999]. Several northwest trending thrust-bounded ranges abut the ATF east of 95°E. The Qilian Shan Front is the easternmost of these ranges and is terminated by the ATF near 40°N, 97°E. Smaller uplifts are present east of the Qilian Shan, where the surface trace of the ATF vanishes into the Gobi Desert. As described above, the rate of slip on the Altyn Tagh Fault is an important quantity in dynamic models of the India-Asia collision. Geodynamic models with a high slip rate on the ATF predict significant crustal extrusion as the mechanism for accommodating north-south convergence in Tibet. In contrast, low slip rates imply that convergence must be accommodated by north-south compression within the Tibetan Plateau. However, the slip rate on the Altyn Tagh Fault is not well determined. Geological studies have estimated Quaternary slip rates at 20−30 mm/yr, indicating that the Altyn Tagh Fault is absorbing a significant amount of the Indo-Asian convergence [*Meriaux et al.*, 2000; *Peltzer et al.*, 1989]. These studies are in disagreement with geodetic investigations which report slip rates of less than 10 mm/yr, implying that crustal thickening is the dominant process accommodating convergence [*Bendick et al.*, 2000, *Rong and Jackson*, 2000].

Investigating the style and geometry of thrusting provides another measure of the amount of convergence that has occurred in northeast Tibet. Geological map-

ping in the forelands of the Dang He Nan Shan, Daxue Shan, and Qilian Shan suggests that these ranges are the surface expression of a series of asymmetric ramp anticlines that are flanked by thrust faults, which bottom out into a midcrustal décollement [*Meyer et al.*, 1998]. This mapping has allowed the rate of late Cenozoic convergence in NE Tibet to be estimated at 15 mm/yr. However, these estimates are based upon many assumptions about the subsurface structure of the foreland thrusts systems. Through magnetotelluric imaging of the Daxue Shan foreland we present an independent estimate of the rate of convergence across the North Hills and Chang Ma thrusts and its implications for Indo-Asian convergence.

2. Magnetotelluric Data Collection and Analysis

Magnetotelluric (MT) surveys have been previously used to study crustal and mantle structure in southern Tibet [*Chen et al.*, 1996; *Van Ngoc et al.*, 1986]. To date, the only MT data collected in northern Tibet has been for oil and mineral exploration. This includes the study of *Zhu and Hu* [1995] and the data presented in this paper.

In 1995-1996, broadband MT data were collected on three profiles that crossed the eastern segment of the Altyn Tagh Fault (lines W1-W3 in Plate 1). Data were also collected on line E1 that crosses the foreland of the Daxue Shan. These data were acquired for China National State Petroleum Corporation. The sedimentary basins north of the Altyn Tagh Fault were the primary target of these surveys, and thus the profiles cross the Altyn Tagh Fault asymmetrically. Data were collected with an Electromagnetic Instruments MT-1 broadband magnetotelluric system. No remote reference was used, so spatially localized noise cannot be removed from the data. However, the lack of cultural noise and ground motion generally ensured good data quality without the use of a remote reference. Electric and magnetic field variations were recorded in the frequency range of 300-0.001 Hz. These time variations were then Fourier transformed to give estimates of the impedance in the frequency domain [*Vozoff*, 1991].

The tensor decomposition scheme of *Chave and Smith* [1994] was used to determine the dimensionality of the data. A relatively consistent geoelectric strike direction was found for all the lines that justified the application of two-dimensional magnetotelluric interpretation. Using such an interpretation, MT data can be separated into two modes, the transverse magnetic (TM) mode in which electric currents flow along the profile and the transverse electric (TE) mode in which electric currents flow across or perpendicular to the profile [*Vozoff*, 1991]. It has been shown that in cases where the subsurface resistivity structure is three-dimensional, the TM mode data can be more reliably interpreted with a two-dimensional (2-D) model than the TE mode [*Wannamaker et al.*, 1984]. Where possible, models consistent with both modes of the data were computed; however, for many of the lines considered in this paper, only the TM data have been considered. On each profile the MT data (frequency-dependent apparent resistivity and phase) were converted into electrical resistivity as a function of depth using two different inversion algorithms: (1) the minimum structure inversion (RRI) of *Smith and Booker* [1991] which generates the smoothest model that fits the data and (2) a variant of the conjugate gradient inversion of *Mackie and Madden* [1993] which generates a smooth model closest to an a priori model while still fitting the data. The a priori model chosen for all such inversions is a 100 Ω m half-space. This choice of an priori model is clearly not important, since inversions starting from several different a priori models gave very similar results. As the models resulting from the two inversion algorithms show close agreement, only one model is shown.

3. Eastern Line

Line E1 is 85 km in length with an average site spacing of 3 km, and its southern part is located within the foreland of the Daxue Shan. Farther north, the line crosses the intersection of the ATF and the northern terminus of the Qilian Shan, a Paleozoic fold belt consisting of highly metamorphosed clastic and volcanic rocks, believed to be the basement of the Hexi Corridor to the north. Several Cenozoic and Mesozoic sedimentary basins are found between the Daxue Shan and the Qilian Shan.

A well-defined geoelectric strike of N135°E was determined from the data for line E1 and is in agreement with the geological strike of the thrust ranges. The impedance data were rotated to this strike direction, and the apparent resistivity and phase were calculated. Plate 2 shows the apparent resistivity and phase pseudosections for line E1. Plotting the data in this format gives an impression of the variation of apparent resistivity with depth, since penetration depth increases as frequency decreases. Lateral changes in the apparent resistivity (Plate 2a) at high frequencies correlate with the geological units mapped at the surface [*Bureau of Geology and Mineral Resources of Gansu Province*, 1984]. Metamorphosed volcanics and clastics appear as resistive units, while Quaternary sediments coincide with the lower resistivities [*Palacky*, 1987]. Two southwest dipping low-resistivity features (C1) are seen in the range of frequencies from 300 to 1 Hz. In addition, a sharp vertical contrast in the apparent resistivity (from 1000 Ω m to 10 Ω m) is imaged ~20 km from the NE end of the line throughout most of the frequency range.

To convert the MT data into a model of resistivity

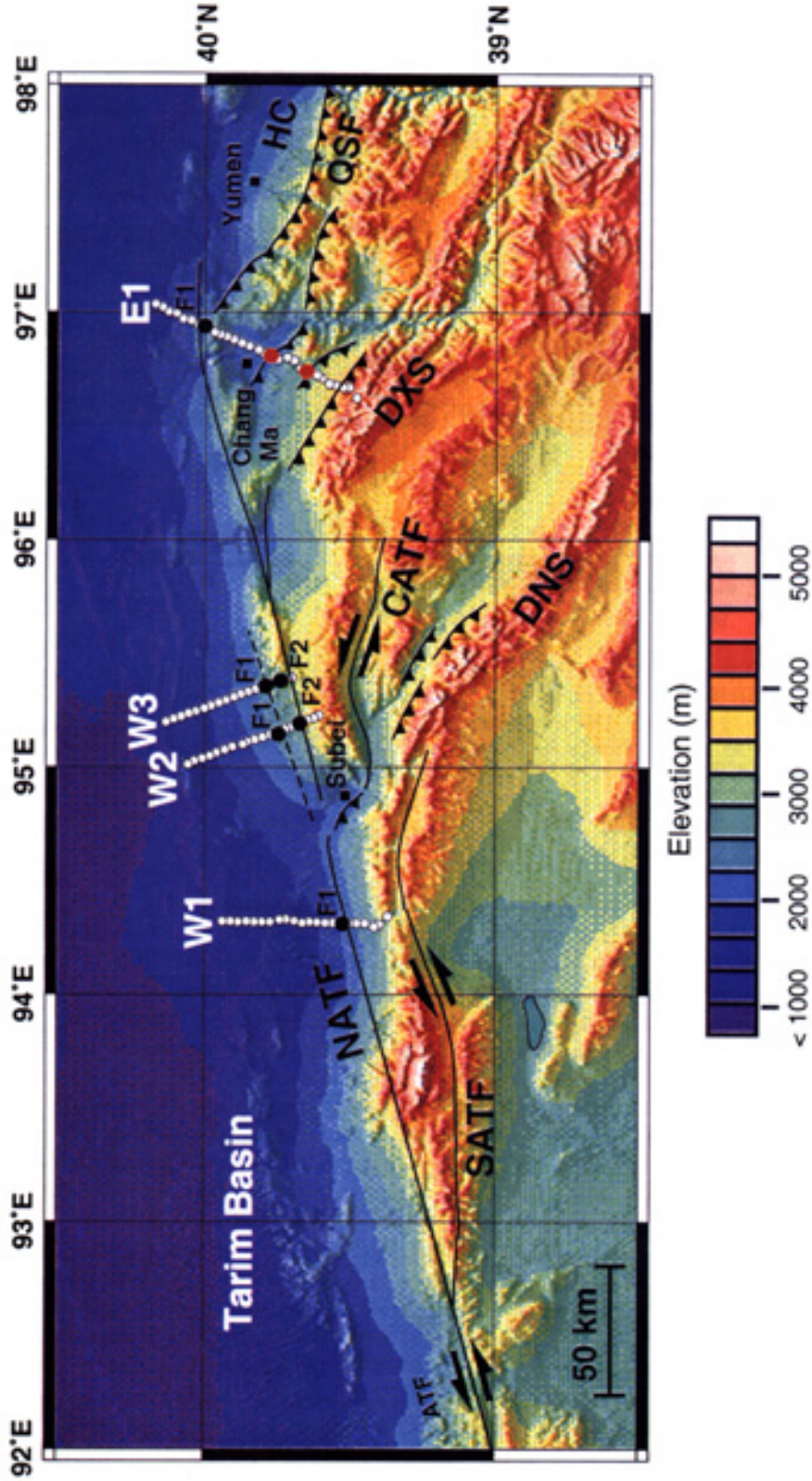

Plate 1. Locations of magnetotelluric (MT) profiles and regional faulting. Fault traces adapted from *Meyer et al.* [1998, Figure 10b] and *Wang* [1997, Figure 2]. Black circles indicate location of the Altyn Tagh Fault based on MT data; labels F1 and F2 are discussed in the text. Red circles indicate thrust fault locations. Abbreviations are as follows: CATF, Central Altyn Tagh Fault; SATF, South Altyn Tagh Fault; and NATF, North Altyn Tagh Fault. Thrust ranges are labeled as in Figure 1. Topography is from the *EROS Data Center* [1993]

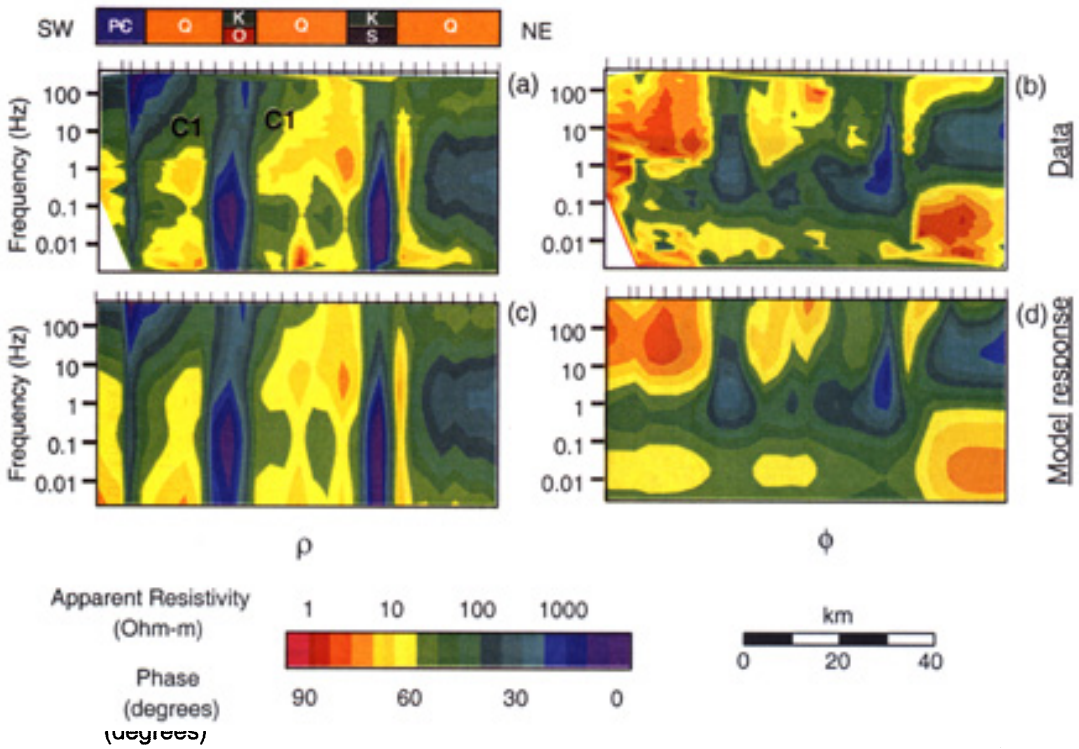

Plate 2. Transverse magnetic (TM) mode data for line E1 and the corresponding model response: (a) TM apparent resistivity, (b) TM phase, (c) TM mode apparent resistivity response of the model shown in Plate 3, and (d) TM mode phase response of the model shown in Plate 3. Geological units are based upon *Bureau of Geology and Mineral Resources of Gansu Province* [1984]. Vertical ticks indicate location of MT sites. Label C1 is discussed in text. Overall RMS misfit is 2.8.

as a function of depth, the 2-D inversion algorithms described in section 2 were used. The model in Plate 3 is the result of a combined mode (TM and TE), conjugate gradient inversion. The overall root-mean-square (RMS) misfit (ϵ_R) of the model is 2.8. The RMS misfit gives an estimate of how well a given model fits the data. It is defined as the square root of the reduced χ^2, which, in turn, is related to the ratio of the residuals (data minus model response) to the standard error in the data. Given data with normally distributed errors, the most probable value of χ^2 occurs when the RMS misfit equals unity. The fit to the data can be seen visually in Plates 2c and 2d, where the apparent resistivity and phase response of the model in Plate 3 are shown. Note the similarity between data and model response.

The most striking features of the models in Plate 3 are the two southwest dipping conductive zones (C1) on the NE flank of the Daxue Shan. The sharp boundaries between the conductive zones and the resistive units above are interpreted as thrust faults which are inverting the sedimentary basins to the NE. This emplaces conductive, Quaternary sediments beneath more competent, resistive units. The continuation of these boundaries to the surface coincides with mapped traces of the Chang Ma and North Hills thrust faults. The dips of the conductive zones associated with the North Hills and Chang Ma thrusts equal $9° \pm 2°$ and $13° \pm 1°$, respectively. These dips are relative to the ground surface, having allowed for a topographic slope of $\sim 2°$. The MT data are sensitive to structure at depths up to ~ 8 km, but no significant changes in resistivity are detected below $3 - 4$ km. Through forward modeling it was shown that termination of the dipping conductive zones (C1) around $3 - 4$ km depth is required by the data. These dip angles are the averaged results of a series of data inversions in which several parameters were varied. Thus dip angles from 5° to 13° are possible for the North Hills thrust, while angles of $11° - 15°$ are permitted for the Chang Ma thrust.

Consider first the southernmost conductive zone, where the dipping resistivity boundary projects to the surface trace of the North Hills thrust. A simple explanation would be that this boundary is a low-angle thrust ramp extending to a depth of several kilometers. However, two external observations lead us to believe

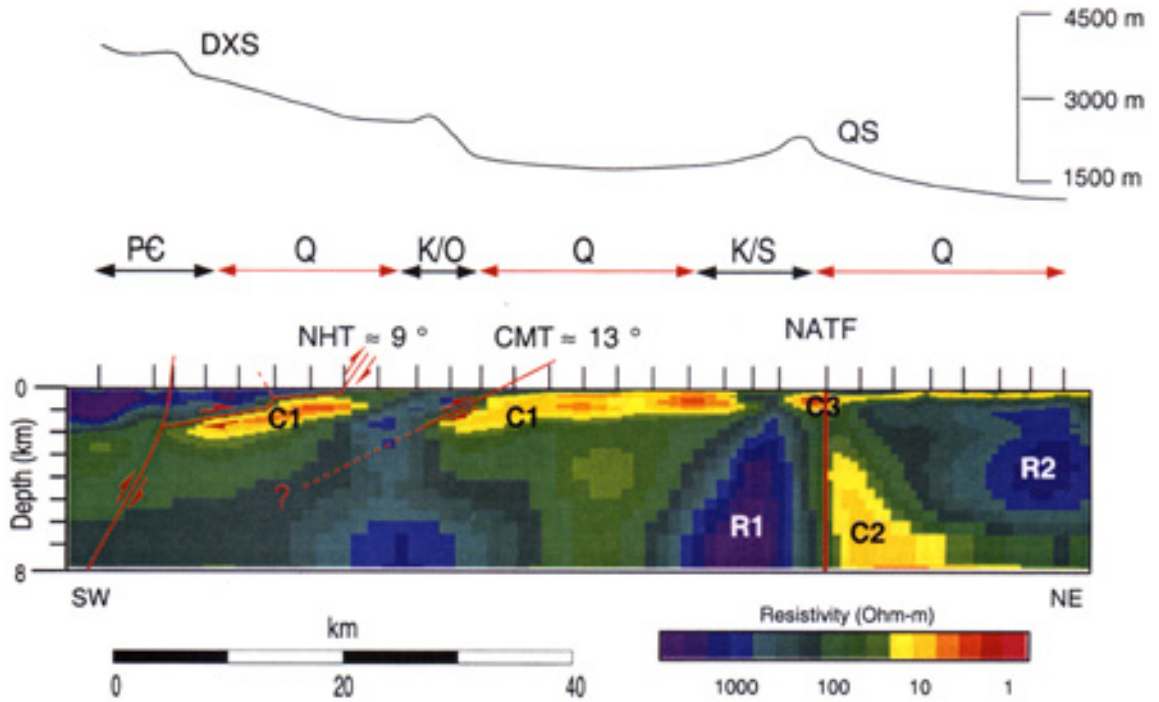

Plate 3. Resistivity model of line E1, with vertical exaggeration 2:1. Model is produced by a conjugate gradient, transverse magnetic and transverse electric mode inversion model; RMS misfit is 2.8. Labeled features are discussed in the text. Vertical ticks indicate location of MT sites. Abbreviations are as follows: DXS, Daxue Shan; QS, Qilian Shan; NHT, North Hills Thrust; CMT, Chang Ma thrust; NATF, North Altyn Tagh Fault. Geological units are from *Bureau of Geology and Mineral Resources of Gansu Province* [1984]. Topography is from *Defense Mapping Agency* [1989].

that what is imaged is a flat associated with a progressive ramp-flat thrust system that has propagated from the primary range thrust into the foreland of the Daxue Shan.

(a) First, geological and geophysical studies in this area give indications of steeper dips at the surface in this area. For example, surface dips in the Liupan Shan, to the east of Gansu, range between 40° and 60° [*Zhang et al.*, 1991]. Seismic reflection studies across the Arlar Fault in the foreland of the Qimantag Shan also image a steep dip in the near surface [*Song and Wang*, 1993].

(b) Second, there is evidence that progressive ramp-flat thrusting is occurring in the region. *Wu et al.* [1995] seismically imaged a series of thrust faults that could be traced down to subhorizontal reflectors in the foreland of the Qilian Shan. This sequence of faults progressively steps to shallower depths moving into the foreland. In addition, *Meyer et al.* [1998] propose that the North Hills thrust is a steep ramp that bottoms into a shallow, SW dipping flat at around 1 km depth beneath the North Hills anticline. Good agreement is evident when the fault geometry of *Meyer et al.* [1998] is compared to the resistivity model in Plate 3.

The nature of the Chang Ma thrust system is less clear. In common with the primary range thrusts of the Qilian Shan, Daxue Shan, and Dang He Nan Shan the Chang Ma thrust emplaces Paleozoic rock in the hanging wall upon Quaternary sediments. However, unlike these major thrusts and similar to the North Hills thrust, the (northern) Chang Ma thrust has not produced significant uplift. Additionally, we have constrained the dip of thrusting in the upper 2 km to be $13° \pm 1°$. A model that extends this fault to depth must agree with both the observed near-surface dip and the lack of significant uplift SW of the fault. Thus, in the absence of further constraints, the simplest explanation is that the Chang Ma thrust projects from the surface at a shallow angle into the hinterland, joining up with the primary range thrust of the Daxue Shan. Regrettably, the commercial MT profile did not adequately cross this primary range thrust.

Are there other explanations for these dipping conductive zones? One alternative would be if they were due to an aquifer. Though such aquifers sometimes exhibit small gradients ($\sim 2°$), the more steeply dipping zones imaged cannot be readily accounted for in this manner. Thus it is more likely that they are due to underthrust sediments.

The Altyn Tagh Fault is expressed as a near vertical resistivity contrast that reaches the surface on the

northeast flank of the Qilian Shan. The shallow structure of the fault zone appears to be conductive (C3). This is similar to the San Andreas Fault near Parkfield, where the conductive fault zone is due to fracturing in the damaged zone of the fault [*Unsworth et al.*, 1997]. However, the site spacing in the present study is too large to adequately image such fine-scale structures.

Southwest of the ATF is a resistive unit, R1, which extends to the southwest end of the profile and is believed to be Precambrian basement. Note that this unit comes close to the surface at two topographic highs along the profile, one along the hanging wall of the Chang Ma thrust and the other underneath the Qilian Shan. Northeast of the ATF, resistive feature R2 is interpreted to be the Precambrian basement beneath the Tarim Basin. Features R1 and R2 on either side of the ATF show little structure and appear to extend to a depth of at least 8 km. The geometry of the conductive zone (C2) northeast of the fault is not easily explained by the present northeast vergence of the region. The northeastern margin of this zone is terminated by a north dipping contact with the basement. It could possibly be related to the junction of the ATF and the Qilian Shan thrust, although this is unlikely as this conductive zone is also imaged on all three of the western lines which cross the ATF far from the junction. A more detailed discussion of this feature is presented in section 5.

4. Western Lines

Lines W1 through W3 extend from the northern flank of the Altyn Shan into the Tarim Basin. Tensor decomposition yields a geoelectric strike parallel to the Altyn Tagh Fault (N60° – 70°E). Further justification for a 2-D interpretation of the data is evident in the phase data for the three western lines (Plate 4). The broad similarities both along the profiles and with decreasing frequency give qualitative evidence for a 2-D structure in the western region. Resistivity models for lines W1-W3 are shown in Plate 5 and were produced by conjugate gradient inversion of TM mode data. The data on all lines are sensitive to structure to a depth of 8 km, but structure at the ends of the profiles is not well constrained by the data. The RMS misfits for the models of lines W1 through W3 are 2.5, 1.9, and 2.4, respectively, and represent adequate, but not ideal, fits to the TM mode data. The presence of multiple profiles allows us to investigate structural variations along the Altyn Tagh Fault.

Initially, resistivity structure common to all three profiles is examined. A region of high conductivity (C1) is seen at the surface in all models, extending to a depth of $\sim$1.5 km. This probably consists of conductive Quaternary alluvium transported northward from the Altyn Shan in agreement with geological mapping in the region and shallow bore holes [*Bureau of Geology and Mineral Resources of Gansu Province*, 1984]. The sediment cover appears thickest where the north slope of the Altyn Shan begins to shallow ($\sim 10 - 15$ km from the south end of the profiles).

A vertical resistivity contrast (F1) is evident crossing from the resistive unit (R1) to the south into the conductive region (C2) to the north. This contrast extends to depths of at least 8 km on all lines and is coincident with the surface trace of the North Altyn Tagh Fault (NATF) on line W1 (Plate 1). Just south of the ATF, resistive unit R1 extends to depth beneath the Altyn Shan. To the north of the ATF, crystalline Precambrian basement (R2) is imaged beneath the sediments of the Tarim Basin. The top of this unit is seen to rise to the surface near the north end of the lines, where Precambrian outcrops have been mapped [*Bureau of Geology and Mineral Resources of Gansu Province*, 1984]. Finally, a conductive zone C2 is present north of the ATF in all models. This is believed to be the same feature present in the eastern line model (C2, Plate 3). On all lines studied, this feature is terminated on the southern side by the ATF and to the north is overlain by resistive material along a north dipping contact.

Several along-strike structural variations are observed on these western lines. The conductor C2 increases both in strength and depth moving to the east. On line W1 the zone is well localized, and the lowest resistivity is $\sim$50 Ω m, whereas to the east a broad region of 10 Ω m is imaged on lines W3 and E1. Possible origins of this conductor are discussed in section 5.

Most striking is the presence of an abrupt change in lateral resistivity (F2) to the south of F1 on lines W2 and W3. This contact is in line with the surface trace of the NATF in the region. Fault F1 is structurally similar on all of the western lines; however, to the east of Subei, F1 is located $6 - 10$ km north of the mapped trace of the eastern NATF (Plate 1). Line W3 also shows a thrust fault (F3) which reaches the surface just south of F2. A hint of this fault is present in line W2, but again, structure is not well constrained at the ends of the lines.

5. Discussion

5.1. Regional Thrusting

Crustal-scale thrusting and basin infilling are believed to have raised the northeast margin of the plateau to its present elevation and may continue to build the plateau northward and eastward [*Chen et al.*, 1999; *Meyer et al.*, 1998; *Tapponnier et al.*, 1990; *Burchfiel et al.*, 1989]. Can the resistivity models presented here clarify details of this process?

The low angles ($< 20°$) of the faults imaged on line E1 imply that a considerable amount of shortening may be taken up by the North Hills and Chang Ma thrusts.

The minimum cumulative shortening on these thrusts can be estimated by measuring the horizontal distance which the conductive sediments have been underthrust beneath the ranges to the southwest. It should be emphasized that this approach gives a minimum estimate; when sediments are thrust to depth, they are compressed and become more resistive [*Palacky,* 1987]. Thus once the sediments have been sufficiently compacted, they cannot be distinguished from other rock units. This limits the estimate of the total horizontal extent of emplacement. This analysis yields horizontal displacements of 14 km and 7 km on the North Hills and Chang Ma thrusts, respectively.

Similar horizontal offsets have been found by *Xu et al.* [1989] in the foreland of the Qilian Shan, where Paleozoic rocks have been thrust 5–10 km over Cretaceous and Tertiary sediments of the Hexi Corridor. Assuming that similar offsets have occurred on all the major thrusts identified in the region, more than 100 km of shortening may have been accommodated between the Dang He Nan Shan and the Qilian Shan. Such shortening is consistent with the amount of late Cenozoic shortening in the region estimated from isostatic modeling [*Meyer et al.,* 1998]. In order to assess the rates of convergence and uplift in these ranges it is necessary to establish the date at which thrusting began. Three lines of evidence point to this occurring around 5 Ma.

1. A significant increase in the sedimentation rate between 5 and 6 Ma is evident in the Yumen drill hole [*Gansu Geological Bureau,* 1975]. This well is located in a foreland basin of the Qilian Shan, and the rapid increase in sedimentation probably reflects the onset of regional thrusting and mountain building [*Meyer et al.,* 1998].

2. Holocene slip rates show that 5 ± 1.3 Myr is sufficient time to produce the late Cenozoic relief observed in the Daxue Shan [*Meyer et al.,* 1998].

3. *Métivier et al.* [1998] reconstructed the depositional history of the Qaidam basin based on drill logs and isopach maps and indicated that a sharp increase in accumulation rate occurred at the beginning of the Pliocene (5.3 Ma). This may well have been the result of basin closure as the ranges to the north began to rise.

Assuming a date of 5.5 Ma for the onset of thrusting, the minimum convergence on the North Hills and Chang Ma thrusts yield slip rates of 2.5 mm/yr and 1.3 mm/yr, respectively. Projecting the shortening on these two thrusts onto the ATF gives ~ 3 mm/yr of left-lateral slip between 96°E and 97°E. This is broadly in agreement with the 4 ± 2 mm/yr of slip estimated by *Meyer et al.* [1996]. It is stressed that these rates are minimum convergence rates as the amount of convergence estimated is a lower bound. Additionally, the onset of thrusting at 5.5 Ma is an upper bound as this most likely represents the initiation of the range front thrust which subsequently propagated into the foreland.

Combining the convergence rates and dips observed on the North Hills flat and Chang Ma thrust, we arrive at uplift rates of 0.4 mm/yr and 0.3 mm/yr, respectively. Such rates predict late Cenozoic uplifts of 2.2 km and 1.6 km on the North Hills and Chang Ma systems. These uplifts are in rough agreement with the moderate topography of the foreland but are significantly less than that seen in the Qilian Shan, Daxue Shan, and Dang He Nan Shan. This probably indicates that the primary ramp thrusts to the south are steeper than the foreland thrust systems imaged by the MT data.

To relate convergence in the Daxue Shan foreland to the measured slip rates on the central and eastern Altyn Tagh Fault, the convergence rates for the North Hills and Chang Ma thrusts are used to determine a cumulative rate of convergence for the region between the Dang He Nan Shan and the Qilian Shan. Making some gross simplifications, the thrusting in the region can be represented by three sets of foreland thrusts, each propagating back into a steep ($\sim 45°$) range thrust. Slip rates on these thrusts are estimated to be the average of those measured on the Chang Ma and North Hills thrusts. This geometry gives rise to a minimum regional convergence rate of 11 mm/yr parallel to the Altyn Tagh Fault.

As the ATF nears its eastern terminus, strike-slip motion is progressively transferred to the thrust faults south of the fault [*Burchfiel et al.,* 1989; *Meyer et al.,* 1996; *Bayasgalan et al.,* 1999]. This results in a decrease in slip rate from its maximum on the central ATF to zero as the surface trace of the ATF vanishes. Geodetic slip rates of < 10 mm/yr on the central Altyn Tagh Fault imply a slip rate at the eastern end of the fault much lower than the minimum estimate derived in this paper. Thus the estimate of the regional slip rate on the eastern Altyn Tagh Fault derived in this paper is most consistent with geological observations of high slip rates ($20 - 30$ mm/yr) on the central Altyn Tagh Fault, as estimated by *Peltzer et al.* [1989] and others.

5.2. Structure of the Altyn Tagh Fault

A significant resistivity contrast across the NATF was described in section 3. On all the MT profiles analyzed, the conductive zone north of the fault (C2 on Plates 3 and 5) extends from the surface to a depth of at least 8 km. The resistivity of this zone varies between 10 Ω m and 100 Ω m, significantly more conductive than the ~ 1000 Ω m region on either side.

Forward modeling of line E1 showed that this conductive zone is required by multiple sites (Plate 6). The MT response at two sites is shown and allows comparison of the data, the response of the model shown in Plate 3, and the response of this same model with C2 replaced by a uniform 500 Ω m region. The more resistive model is what might be expected if the NATF was bounded by crystalline basement rock on both sides. The fit to the

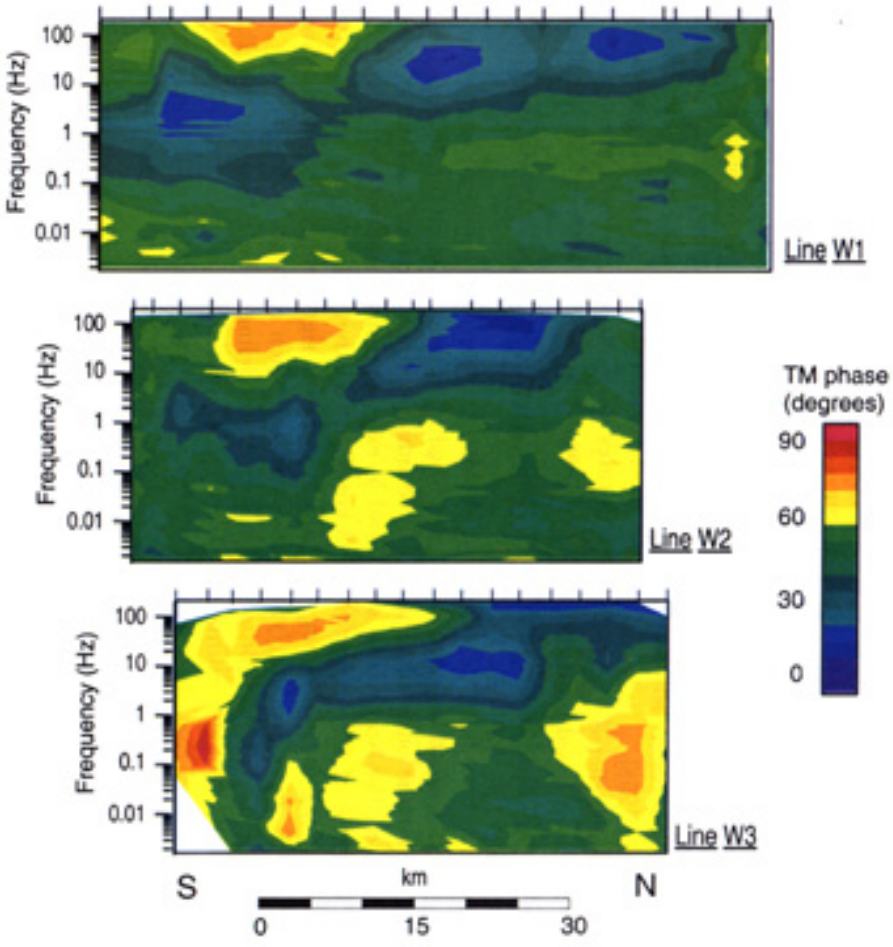

Plate 4. Phase pseudosections for lines W1-W3. High phases are shown in red and yellow, while low phases are shown in blue. Vertical ticks indicate location of MT sites. Note that similar features are seen on all three lines.

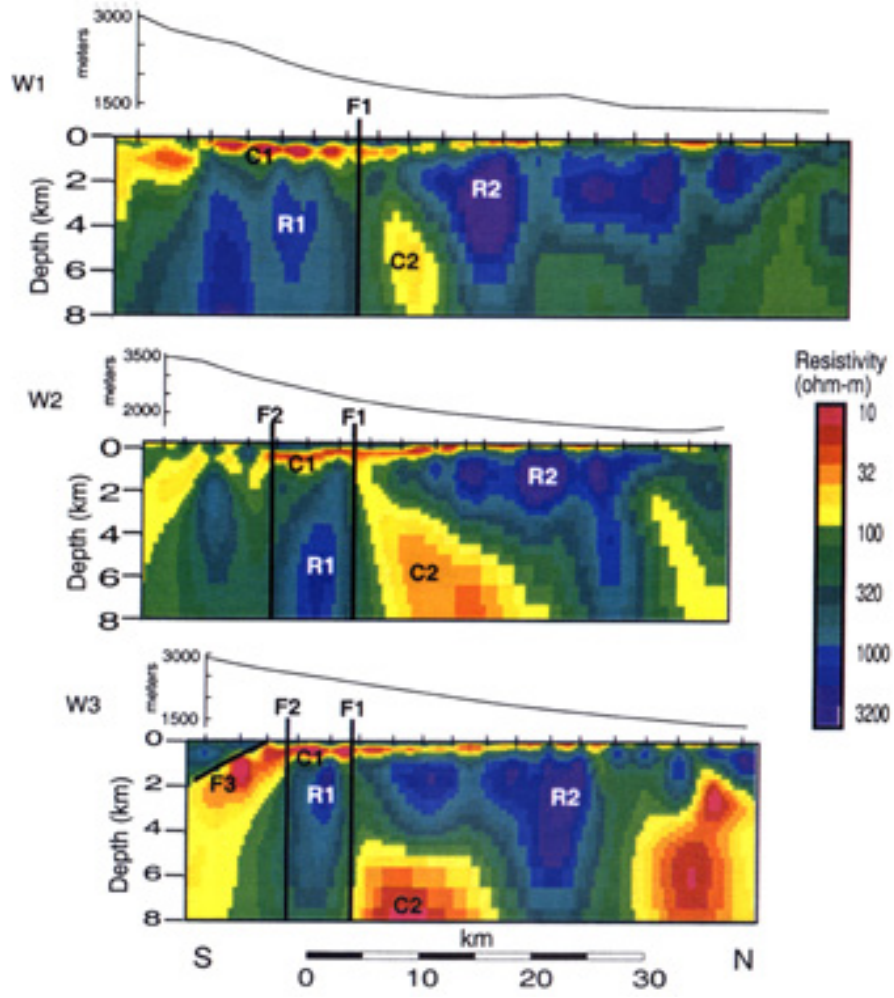

Plate 5. Resistivity models for lines W1-W3. Vertical exaggeration is 2:1. Vertical ticks indicate location of MT sites. Labeled features are discussed in the text. C1, C2, R1, R2, and F1 are common to all lines; F2 is common to lines W2 and W3, and F3 is only clearly imaged on line W3. Topography is from *Defense Mapping Agency* [1989].

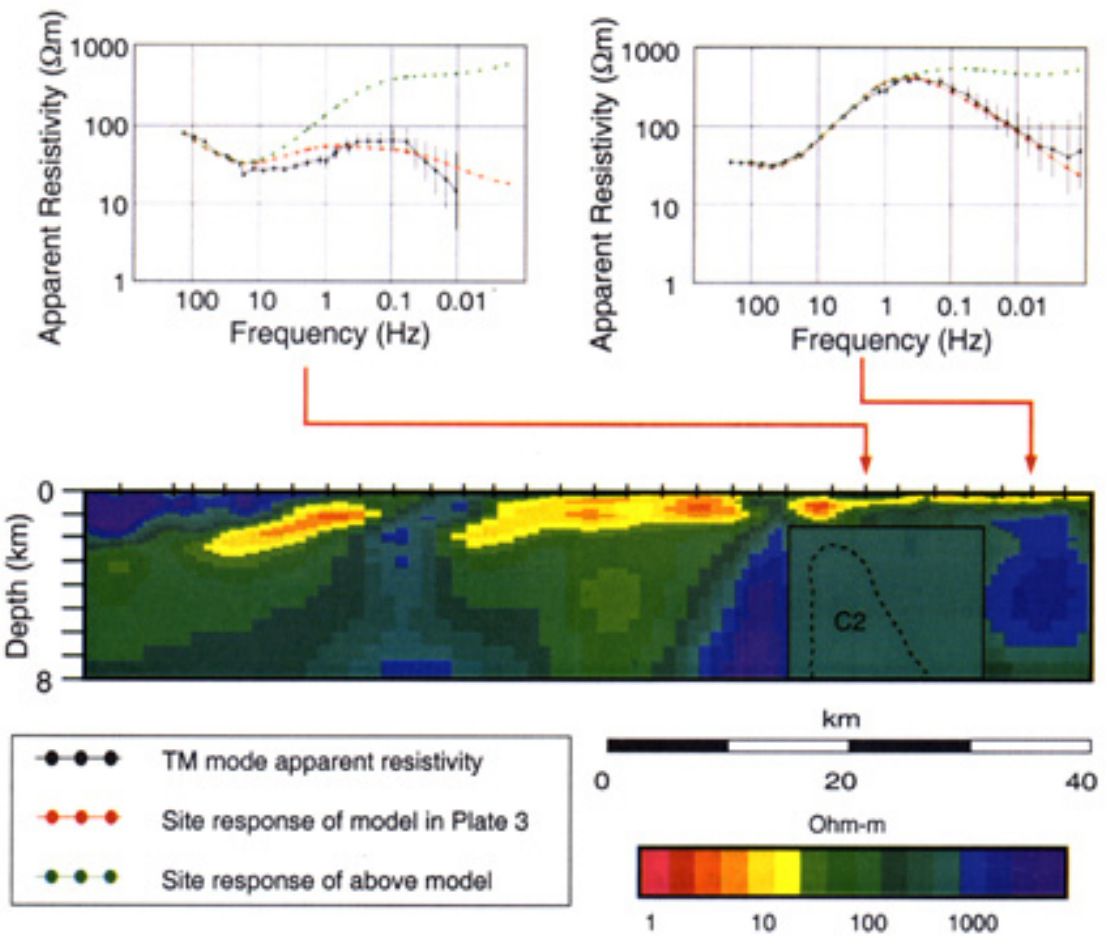

Plate 6. Apparent resistivity data and site response for the model shown in Plate 3 upon modification. Conductor C2 (Plate 3) has been replaced by a 500 Ω m region north of the ATF. Black curves represent TM mode apparent resistivity, green curves show the response of the model shown in Plate 3, and red curves show the response of the modified model. Vertical exaggeration is 2:1.

data for the more resistive model is considerably worse than that obtained with the conductor. The RMS misfit for the resistive model is 5.1, almost twice that of the model with conductive zone present.

An explanation for the cause of the high conductivity is suggested by the geometry of the north dipping contact between C2 and R2. With the northeast vergence of this region such a contact does not appear to be consistent with the present tectonics; that is, it cannot be an active thrust fault. Is it possible that this structure is a relic of a previous orogeny? A series of faults and folds are present north of the Altyn Tagh Fault between 92°E and 96°E [*Bureau of Geology and Mineral Resources of Gansu Province*, 1984]. These long-wavelength (30 – 60 km) folds are aligned parallel to the ATF and expose a Precambrian core. Additionally, pillow lavas and high-pressure metamorphic rocks within the Altyn Tagh near 92° give evidence for a mid-Paleozoic suture [*Sobel and Arnaud*, 1999]. These features hint at north-south compressive events in the past and suggest that the ATF may have activated along this Paleozoic suture. While *Sobel and Arnaud* [1999] give evidence for southward subduction in the Paleozoic, *Yin and Nie* [1996] have proposed that this subduction zone was north dipping. The combination of marine sediments and possibly graphite can make a suture zone electrically conductive [*Shankland and Ander*, 1983]. MT surveys have imaged middle to lower crustal conductors beneath sutures as old as 300–400 Ma [*Santos et al.*, 1999; *Banks et al.*, 1996; *Park et al.*, 1991]. This provides one possible explanation for the zone of enhanced conductivity north of the Altyn Tagh Fault.

The possibility that the ATF formed by reactivating a suture zone is relevant to the debate over the depth extent of the ATF. It has been suggested that the Altyn Tagh Fault extends through the entire lithosphere [*Tapponnier et al.*, 1990; *Wittlinger et al.*, 1998; *Herquel et al.*, 1999]. This information, combined with

the high slip rate on the ATF, implies that a significant amount of north-south convergence is absorbed through the eastward extrusion of the Tibetan lithosphere. *Burchfiel et al.* [1989] and *Burchfiel and Royden* [1991] have argued that the ATF is confined to the upper crust, implying that no crustal material has been extruded beyond the Tibetan Plateau. While our resistivity models do not extend deep enough to directly address this question, if the conductive zone C2 is indeed the signature of a suture, then a lithospheric scale fault is reasonable given the preexisting zone of weakness that probably extends to significant depth. Thus, on the basis of the geological and geophysical evidence to date we prefer a model in which the Altyn Tagh Fault cuts the lithosphere, having activated along a Paleozoic suture. Given this model and the estimated high slip rates, our data support fast eastward extrusion of the Tibetan lithosphere.

5.3. Regional Geometry of the Altyn Tagh Fault

Plate 1 shows the major faults in the region considered by this study. East of 93°E, the ATF consists of two en echelon segments, the north and south ATF (NATF and SATF). Near Subei ($\sim$ 95°E) the NATF bends, changing strike from N70°E to N75°E. The SATF bends to the southeast here, forming the northern boundary of the Qaidam basin. Also, at this point a third strand, the central Altyn Tagh Fault (CATF), branches to the east [*Wang*, 1997]. Farther east, the SATF and CATF follow the trend of the Dang He Nan Shan and Daxue Shan, respectively, while the NATF vanishes into the desert.

By tracing the distinctive electrical signature of the region north of the Altyn Tagh Fault (C2), the NATF can be mapped on either side of the asperity near Subei. The surface trace of the NATF is in close agreement with the fault locations defined by our resistivity models (F1 on line W1 and F2 on lines W2-W3). A sliver of Precambrian rock ($\sim$10 km wide) has been mapped between 95°E and 96°E, bounded to the south by the NATF and to the north by a thrust fault [*Bureau of Geology and Mineral Resources of Gansu Province*, 1984]. The location of this thrust is coincident with fault F1 on lines W2 and W3. While this fault may exhibit a component of thrusting, the fact that the contacts are near vertical and extend to depths beyond 8 km can be explained by extending the western segment of the NATF to the east of Subei (Plate 1). The two segments of the NATF bound a thin (6 – 10 km wide) fault block to the east of Subei that is imaged on lines W2 and W3 (Plate 5). It is not clear from the present study if the western segment of the NATF extends beyond 95°30′E.

5.4. Lithospheric Décollement

Geological mapping, neotectonic studies, and SPOT image analysis suggest that the numerous thrusts in this region coalesce into a midcrustal décollement [*Peltzer et al.*, 1989; *Meyer et al.*, 1996, 1998]. The magnetotelluric data presented in this paper give no direct evidence to either support or refute the existence of such a detachment. While the MT data are sensitive to the depths at which such a feature has been postulated, there is no requirement that a contrast in electrical resistivity would accompany such a feature. The absence of resistivity variations below 3 – 4 km may simply indicate that at these depths the thrust faults have resistive crystalline rock in both the footwall and hanging wall. We are also unable to address the model of lithospheric subduction beneath the Kunlun Shan [*Tapponnier et al.*, 1990], as we have not imaged the décollement required by this model.

6. Conclusions

Analysis of broadband magnetotelluric data has provided subsurface images of strike-slip and thrust faults in the northeast region of the Tibetan Plateau. This region is undergoing crustal shortening and uplift along a series of thrust faults. Two such faults, the Chang Ma and the North Hills thrusts, are imaged to depths of at least 3 – 4 km with dips of 13° ± 1° and 9° ± 2°, respectively. These thrusts are inverting the basins to the north, emplacing basement rock over sediments. The horizontal extent of the conductive zones implies minimum horizontal shortening of 14 km and 7 km on the North Hills and Chang Ma thrusts, respectively. Assuming an onset of thrusting at 5.5 Ma, this corresponds to minimum convergence rates of 1.3 mm/yr and 2.5 mm/yr on the Chang Ma and North Hills thrusts, respectively. These slip rates correspond to $\sim$3 mm/yr of sinistral slip on the Altyn Tagh Fault between 96°E and 97°E, consistent with the 4 ± 2 mm/yr of slip estimated by geological studies. Extending the convergence estimates to include thrusting in the surrounding ranges implies a minimum of 11 mm/yr of shortening parallel to the Altyn Tagh Fault between the Dang He Nan Shan and Qilian Shan. Both the style of thrusting and rate of shortening are in agreement with geologic studies of the region and favor relatively fast movement on the Altyn Tagh Fault. This implies that eastward extrusion of the Tibetan lithosphere is accommodating a significant amount of the convergence between India and Asia.

Four magnetotelluric profiles have imaged the North Altyn Tagh Fault as a vertical feature to a depth of at least 8 km. An additional crustal scale fault, believed

to be an extension of the western segment of the NATF, has been identified ~6–10 km north of the surface trace of the eastern NATF. North of the NATF, a conductive zone has been imaged that may be the expression of a suture zone.

Acknowledgments. We are grateful for permission from CNSPC to publish these data. We thank Darrel Cowan, Peter Molnar, and Steve Thompson for helpful discussions. This paper has benefited greatly from reviews by An Yin, Phil Wannamaker, and Craig Jones.

References

Allègre, C.J., et al., Structure and evolution of the Himalaya-Tibet orogenic belt, *Nature, 307,* 17-22, 1984.

Banks, R.J., D. Livelybrooks, P. Jones, and R. Longstaff, Causes of the high crustal conductivity beneath the Iapetus suture zone in Great Britain, *Geophys. J. Int., 124,* 433-455, 1996.

Bayasgalan, A., J. Jackson, J.F. Ritz, and S. Carretier, Field examples of strike-slip fault terminations in Mongolia and their tectonic significance, *Tectonics, 18,* 394-411, 1999.

Bendick, R., R. Bilham, J. Freymueller, K. Larson, and G. Yin, Geodetic evidence for a low slip rate in the Altyn Tagh Fault system, *Nature, 404,* 69-72, 2000.

Burchfiel, B.C., and L.H. Royden, Tectonics of Asia 50 years after the death of Emile Argand, *Eclogae Geol. Helv., 84,* 599-629, 1991.

Burchfiel, B.C., D. Quidong, P. Molnar, L. Royden, W. Yipeng, Z. Peizhen, and Z. Weiqi, Intracrustal detachment within zones of continental deformation, *Geology, 17,* 448-452, 1989.

Bureau of Geology and Mineral Resources of Gansu Province, Tectonic systems map of Gansu province of the People's Republic of China, scale 1:1,500,000, Beijing, 1984.

Chave, A., and J.T. Smith, On electric and magnetic galvanic distortion tensor decompositions, *J. Geophys. Res., 99,* 4669-4682, 1994.

Chen, L., J.R. Booker, A.G. Jones, N. Wu, M.J. Unsworth, W. Wei, and H. Tan, Electrically conductive crust in southern Tibet from INDEPTH magnetotelluric surveying, *Science, 274,* 1694-1696, 1996.

Chen, W.-P., C.-Y. Chen, and J. Nábelek, Present-day deformation of the Qaidam basin with implications for intracontinental tectonics, *Tectonophysics, 305,* 165-181, 1999.

Defense Mapping Agency, Tactical pilotage charts, scale 1:500,000, G-8A, G-8B, F-7C, St. Louis, 1989.

Dewey, J.F., and K.C. Burke, Tibetan, Variscan, and Precambrian basement reactivation: Products of continental collision, *J. Geol., 81,* 683-692, 1973.

Dziewonski, A.M., T.A. Chou, and J.H. Woodhouse, Determination of earthquake source parameters from waveform data for studies of global and regional seismicity, *J. Geophys. Res., 86,* 2825-2852, 1981.

England, P., and G. Houseman, Finite strain calculations of continental deformation, 2., Comparison with the India-Asia collision zone, *J. Geophys. Res., 91,* 3664-3676, 1986.

Gansu Geological Bureau, Geologic map of Gansu, scale 1:1,000,000, Minist. of Geol., Beijing, 1975.

EROS Data Center, GTOPO30 global digital elevation model, map, 30 arc sec resolution, U.S. Geol. Surv., Sioux Falls, 1993.

Herquel, G., P. Tapponnier, G. Wittlinger, J. Mei, and S. Danian, Teleseismic shear wave splitting and lithospheric anisotropy beneath and across the Altyn Tagh Fault, *Geophys. Res. Lett., 26,* 3225-3228, 1999.

Mackie, R.L., and T.R. Madden, Three-dimensional magnetotelluric inversion using conjugate gradients, *Geophys. J. Int., 115,* 215-229, 1993.

Meriaux, A., F.J. Ryerson, P. Tapponnier, J. Van der Woerd, R.C. Finkel, M.W. Caffee, C. Lasserre, X. Xu, H. Li, and Z. Xu, Fast extrusion of the Tibet Plateau: A 3 cm/yr, 100 Kyr slip-rate on the Altyn Tagh Fault (abstract), *Eos. Trans. AGU, 81*(48), Fall Meet. Suppl., T62D-07, 2000.

Métivier, F., Y. Gaudemer, P. Tapponnier, and B. Meyer, Northeastward growth of the Tibet Plateau deduced from balanced reconstruction of two depositional areas: The Qaidam and Hexi Corridor basins, China, *Tectonics, 17,* 823-842, 1998.

Meyer, B., P. Tapponnier, Y. Gaudemer, G. Peltzer, G. Shunmin, and C. Zhitai, Rate of left-lateral movement along the easternmost segment of the Altyn Tagh Fault, east of 96°E (China), *Geophys. J. Int., 124,* 29-44, 1996.

Meyer, B., P. Tapponnier, L. Bourjot, F. Métivier, Y. Gaudemer, G. Peltzer, G. Shunmin, and C. Zhitai, Crustal thickening in Gansu-Qinghai, lithospheric mantle subduction, and oblique, strike-slip controlled growth of the Tibetan Plateau, *Geophys. J. Int., 135,* 1-47, 1998.

Molnar, P., and H. Lyon-Caen, Fault plane solutions of earthquakes and active tectonics of the Tibetan Plateau and its margins, *Geophys. J. R. Astron. Soc., 99,* 123-153, 1989.

Nelson, K., et al., Partially molten middle crust beneath southern Tibet: Synthesis of project INDEPTH results, *Science, 274,* 1684-1688, 1996.

Palacky, G., Resistivity characteristics of geologic targets, in *Electromagnetic Methods in Applied Geophysics,* edited by M.N. Naibighian, pp. 53-129, Soc. of Explor. Geophys., Tulsa, Okla., 1987.

Park, S., G. Biasi, R. Mackie, and T. Madden, Magnetotelluric evidence for crustal suture zones bounding the southern Great Valley, California, *J. Geophys. Res., 96,* 353-376, 1991.

Peltzer, G., and P. Tapponnier, Formation and evolution of strike-slip faults, rifts and basins during the India-Asia collision: An experimental approach, *J. Geophys. Res., 93,* 15,085-15,117, 1988.

Peltzer, G., P. Tapponnier, and R. Armijo, Magnitude of late Quaternary left-lateral displacements along the north edge of Tibet, *Science, 246,* 1285-1289, 1989.

Rong, Y., and D.D. Jackson, Kinematics of Tibetan Plateau from GPS measurements (abstract), *Eos. Trans. AGU, 81*(48), Fall. Meet. Suppl., T22A-03, 2000.

Santos, F.A.M., J. Pous, E.P. Almeida, P. Queralt, A. Marcuello, H. Matias, and L.A.M. Victor, Magnetotelluric survey of the electrical conductivity of the crust across the Ossa Morena zone and South Portugese zone suture, *Tectonophysics, 313,* 449-462, 1999.

Shankland, T.J., and M.E. Ander, Electrical conductivity, temperature, and fluids in the lower crust, *J. Geophys. Res., 88,* 9475-9484, 1983.

Smith, J.T., and J.R. Booker, Rapid inversion of two- and three-dimensional magnetotelluric data, *J. Geophys. Res., 96,* 3905-3922, 1991.

Sobel, E., and N. Arnaud, A possible middle Paleozoic suture in the Altyn Tagh, NW China, *Tectonics, 18,* 64-74, 1999.

Song, T., and X. Wang, Structural styles and stratigraphic patterns of syndepositional faults in a contractional setting: Examples from the Qaidam basin, northwestern China, *AAPG Bull., 77,* 102-117, 1993.

Tapponnier, P., G. Peltzer, A.Y. Le Dain, and R. Armijo, Propagating extrusion tectonics in Asia: New insights from simple experiments with plasticine, *Geology, 10,* 611-615, 1982.

Tapponnier, P., et al., Active thrusting and folding in the Qilian Shan, and decoupling between upper crust and mantle in northeastern Tibet, *Earth Planet. Sci. Lett., 97,* 382-403, 1990.

Unsworth, M.J., P. Malin, G.D. Egbert,

and J.R. Booker, Internal structure of the San Andreas Fault at Parkfield, California, *Geology, 25*. 359-362, 1997.

Van Ngoc, P., D. Boyer, P. Therme, X.-C. Yuan, L. Li, and G.-Y. Jin, Partial melting zones in the crust in southern Tibet from magnetotelluric results, *Nature, 319*, 310-314, 1986.

Vozoff, K., The magnetotelluric method, in *Electromagnetic methods in Applied Geophysics*, edited by M.N. Naibighian, pp. 641-711, Soc. of Explor. Geophys,, Tulsa, Okla., 1991.

Wang, E., Displacement and timing along the northern strand of the Altyn Tagh Fault zone, northern Tibet, *Earth Planet. Sci. Lett., 150*, 55-64, 1997.

Wannamaker, P., G. Hohmann, and S. Ward, Magnetotelluric responses of three-dimensional bodies in layered earths, *Geophysics, 49*, 1517-1533, 1984.

Wittlinger, G., P. Tapponnier, G. Poupinet, J. Mei, S. Danian, G. Herquel, and F. Masson, Tomographic evidence for localized lithospheric shear along the Altyn Tagh Fault, *Science, 282*, 74-76, 1998.

Wu, X.-Z., C.-L. Wu, J. Lu, and J. Wu, Research on the fine crustal structure of the northern Qilian-Hexi corridor by deep seismic reflection, *Acta Geophys. Sin., 38*(SII), 29-35, 1995.

Xu, W., Y. He, and Y. Yan, Tectonic characteristics and hydrocarbons of the Hexi Corridor, in *Chinese Sedimentary Basins*, edited by X. Zhu, pp. 53-62, Elsevier Sci., New York, 1989.

Yin, A., and T.M. Harrison, Geologic evolution of the Himalayan-Tibetan orogen, *Annu. Rev. Earth Planet. Sci., 28*, 211-280, 2000.

Yin, A., and S. Nie, A Phanerozoic palinspastic reconstruction of China and its neighboring regions, in *The Tectonic Evolution of China*, edited by A. Yin and M. Harrison, pp. 442-485, Cambridge Univ. Press, New York, 1996.

Zhang, P., B.C. Burchfiel, P. Molnar, W. Zhang, D. Jiao, Q. Deng, Y. Wang, L. Royden, and F. Song, Amount and style of late Cenozoic deformation in the Liupan Shan area, Ningxia autonomous region, China, *Tectonics, 10*, 1111-1129, 1991.

Zhao, W., et al., Deep seismic reflection evidence for continental underthrusting beneath southern Tibet, *Nature, 366*, 557-559, 1993.

Zhu, R.-X., and X.-Y. Hu, Study of the resistivity structure of the lithosphere along the Golmud-Ejin Qi geoscience transect, *Acta Geophys. Sin., 38*(SII), 46-57, 1995.

P. A. Bedrosian, Geophysics Program, University of Washington, Seattle, WA, 98195. (bedros@geophys.washington.edu)

M. J. Unsworth, Department of Physics, University of Alberta, Edmonton, Alberta, Canada T6G 2J1. (unsworth@Phys.UAlberta.CA)

F. Wang, Beijing Research Institute for Uranium Geology, Beijing, China, 100029. (wf1026@yeah.net)

(received March 15, 2000;
revised January 23, 2001;
accepted April 10, 2001.)